A Time-Split Finite-Volume Algorithm for Three-Dimensional Flowfield Simulation

C. M. Hung* and W. Kordulla†
NASA Ames Research Center, Moffett Field, California

A general finite-volume algorithm is developed for three-dimensional, compressible flow over an arbitrary configuration. The algorithm implements MacCormack's explicit-implicit predictor-corrector scheme in a locally one-dimensional fashion. The code is able to treat problems with a viscous layer in one, two, or all three spatial directions. Calculated results are in very good agreement with the experimental measurements of a blunt-fin induced shock wave/boundary-layer interaction problem. The existence of a horseshoe vortex and two reversed supersonic zones is observed.

Introduction

THE objective of the present paper is to describe the development of a numerical algorithm to solve the three-dimensional, time-dependent, compressible Navier-Stokes equations for high Reynolds number flows over an arbitrary geometry. The essential features of the present algorithm are as follows:

1) It is coded for general three-dimensional body-fitted coordinates.

2) It employs thin-layer approximation in all three spatial directions.

3) It is formulated on the control-volume or finite-volume concept.

4) It implements MacCormack's new explicit-implicit scheme[1] in a time-split fashion.

5) It provides novel, simple starting conditions for blunt bodies.

Computational fluid dynamics has been a revolutionary force recently in practical aerodynamics, e.g., solution of compressible flow at high Reynolds numbers past nonsimple shapes. With the advent of large and fast vectorized computer processors, coding a program in general three-dimensional transformed coordinates is now feasible and is an urgent requirement for three-dimensional flowfield simulations. In high Reynolds number flows, the viscous effects are confined to a thin layer near the wall boundary. The concept of the thin-layer approximation, developed by Baldwin and Lomax,[2] has been tested and validated and is now widely used for various high Reynolds number flow calculations. The validity of the thin-layer approximation in more than one direction has been demonstrated in a previous study of supersonic flow over an axial corner.[3] Extension of the thin-layer approximation to all three directions is straightforward and broadens the scope of the method to more complicated geometries, allowing treatment of wall boundaries in two or all three directions.

The basic idea of the control-volume formulation is easy to understand. Whereas a finite-difference equation is derived via Taylor-series expansions and is consistent over a small region in a limiting sense, the control-volume formulation lends itself to direct physical interpretation. The computational domain is divided into a number of "nonoverlapping" (discussed later) finite volumes surrounding each grid point, and the resulting solution will satisfy the integral conservation laws of mass, momentum, and energy over any group of control volumes and, of course, over the whole computational domain. Hence, the finite-volume formulation does not require a smooth variation of mesh size and in general does not require the volume to be a hexahedron in the three-dimensional case. The advantage of the control-volume formulation is well recognized and it has been widely adopted, for example, Refs. 4 and 5. However, the implementation details differ greatly from one method to another. We employ here a cell concept, rather than a grid-point concept: the corner points of a computation cell are prescribed so that the cell surface areas and volume can be evaluated accurately. In the cell concept, a coordinate transformation is not needed explicitly. This approach also lends itself to a straightforward geometrical interpretation relating the dependent and independent variables in the physical and computational spaces.

An explicit-implicit scheme recently developed by MacCormack[1] incorporates a bidiagonal implicit procedure in the well-proven explicit predictor-corrector method,[6] and has achieved a speed-up of about two orders of magnitude for a shock wave/boundary-layer interaction problem on a flat plate. A brief description of the general finite-volume formulation of MacCormack's explicit-implicit predictor-corrector scheme and a two-dimensional transonic flow computation were presented by Kordulla and MacCormack.[7] Here, we incorporate the thin-layer approximation and employ Strang[8] type time splitting to make the method locally one dimensional for three-dimensional problems. The thin-layer approximation drastically simplifies the evaluation of viscous diffusion and dissipation terms, and allows easy vectorization of the algorithm. This time splitting makes the dependent variables on the right-hand side consistent with the characteristic variables in a similarity transformation and, moreover, requires the use of only one level of dependent variables plus three single arrays, instead of the three levels of dependent variables in MacCormack's scheme.

The case of interaction of a blunt-fin induced shock wave with a turbulent boundary layer is calculated. The results are compared with an experiment[9] conducted at a Mach number of 2.95 with a freestream unit Reynolds number of 6.3×10^7 m^{-1}. The results show very good agreement of surface pressure with measured values at various locations on the fin and on the flat plate.

Presented as Paper 83-1957 at the AIAA 6th Computational Fluid Dynamics Conference, Danvers, Mass., July 13-15, 1983; revision received Feb. 23, 1984. This paper is declared a work of the U.S. Government and therefore is in the public domain.

*Research Scientist, Computational Fluid Dynamics Branch. Member AIAA.

†NRC Senior Research Associate, Computational Fluid Dynamics Branch. Currently with DFVLR Institut fuer Theoretische Stroemungsmechanik, Goettingen, FRG. Member AIAA.

Analysis and Numerical Procedure

Equations in Nondimensional Form

In the absence of body forces and source terms, the governing Navier-Stokes equations for conservation of mass, momentum, and energy in a stationary finite volume $\mathcal{V}$, enclosed by the control surface S, can be written in nondimensional form as

$$\frac{\partial}{\partial t}\int_{\mathcal{V}} \underline{q}\,d\mathcal{V}+\int_S (\underline{qu}+\underline{b})\cdot\underline{n}\,dS=0 \tag{1}$$

where

$$\underline{q}=(\rho,\ \rho u,\ \rho v,\ \rho w,\ \rho E)^T$$

$$E=e_i+\tfrac{1}{2}(u^2+v^2+w^2)$$

$$\underline{b}=(\underline{b}_\rho,\ \underline{b}_m,\ \underline{b}_e)^T,\quad \underline{b}_\rho=0$$

$$\underline{\underline{b}}_m=p\underline{\underline{I}}+M_\infty Re^{-1}\underline{\underline{\tau}}$$

$$\underline{\underline{\tau}}=-\lambda\,\mathrm{div}\ \underline{u}\underline{\underline{I}}-\mu[(\mathrm{grad}\ \underline{u})+(\mathrm{grad}\ \underline{u})^T]$$

$$\underline{b}_e=-\gamma M_\infty (RePr)^{-1}\mu\,\mathrm{grad}\ e_i+p\underline{u}+M_\infty Re^{-1}\underline{\underline{\tau}}\cdot\underline{u}$$

Here, a conventional definition of the flow quantities is used. The Cartesian velocity components (u,v,w) are normalized by the freestream speed of sound a_∞, ρ by ρ_∞, the specific internal energy e_i and total energy E by a_∞^2, and p by $\rho_\infty a_\infty^2$. The viscosity coefficients λ and μ are normalized with respect to the molecular viscosity μ_∞. The constant γ is the ratio of specific heats, Re is the Reynolds number based on freestream velocity, and Pr is the Prandtl number. For a perfect gas the normalized state relations are

$$p=(1/\gamma)\rho T,\qquad e_i=T/\gamma(\gamma-1),\qquad a^2=T$$

where the temperature T is normalized with respect to T_∞.

Equation (1) is a simple expression of the conservation laws, and is valid for a global control volume and also for each local discretized finite-volume cell (i,j,k) shown in Fig. 1. For a notation convention, the superscript without a prime is used for the transformed coordinates [e.g., $x^i=(x^1,x^2,x^3)$ which are interchangeable with (ξ,η,ζ)], and the superscript with a prime is used in the original Cartesian system [e.g., $x^{i'}=(x^{1'},x^{2'},x^{3'})$ which are interchangeable with (x,y,z)]. A similar convention applies to all other vector or tensor quantities. For instance, $u^{i'}=(u^{1'},u^{2'},u^{3'})=(u,v,w)$.

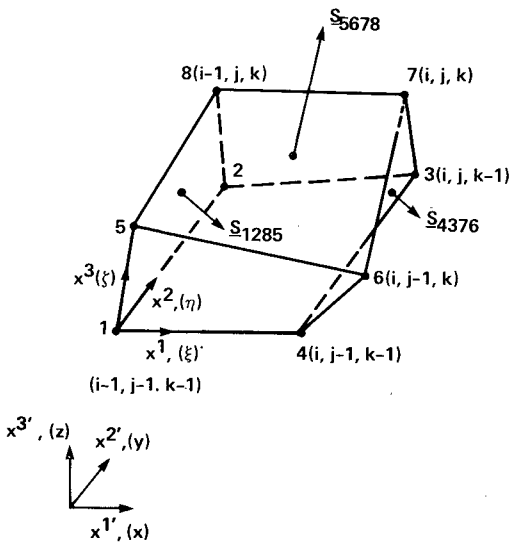

Fig. 1 A hexahedron finite-volume $\mathcal{V}(i,j,k)$ with coordinate systems.

The partial differential equation corresponding to Eq. (1) is

$$\frac{\partial}{\partial t}[\underline{q}(g)^{1/2}]+\frac{\partial}{\partial x^i}[(\underline{qu}+\underline{b})\cdot(g)^{1/2}\underline{g}^i]=0 \tag{2}$$

or

$$\hat{\underline{q}}_{,t}+{}^i\hat{\underline{F}}_{,i}=0$$

where

$$\hat{\underline{q}}\equiv\underline{q}(g)^{1/2},\quad {}^i\hat{\underline{F}}\equiv[(\underline{qu}+\underline{b})\cdot(g)^{1/2}\underline{g}^i]$$

$(g)^{1/2}$ is the Jacobian, and $\underline{g}^i$ is the contravariant base vector in the x^i direction. Here, the Einstein summation convention is used.

Differentiated with respect to time, Eq. (2) becomes

$$\tilde{\underline{q}}_{,t}+({}^i\underline{\underline{\hat{A}}}\tilde{\underline{q}})_{,i}=0,\quad \tilde{\underline{q}}\equiv\hat{\underline{q}}_{,t},\quad {}^i\underline{\underline{\hat{A}}}\equiv\partial^i\hat{\underline{F}}/\partial\hat{\underline{q}} \tag{3}$$

Equation (3) provides the basis for the implicit procedure. Writing Eq. (2) out explicitly, one has

continuity

$$[(g)^{1/2}\rho]_{,t}+[\rho\underline{u}\cdot(g)^{1/2}\underline{g}^\ell]_{,\ell}=0 \tag{4a}$$

momentum for $x^{i'}$ direction

$$[(g)^{1/2}\rho u^{i'}]_{,t}+\Big\{\rho u^{i'}\underline{u}\cdot(g)^{1/2}\underline{g}^\ell+p(g)^{1/2}g^\ell_{(i')}$$
$$-M_\infty Re^{-1}\lambda\frac{\partial u^{n'}}{\partial x^{n'}}(g)^{1/2}g^\ell_{(i')}-M_\infty Re^{-1}$$
$$\times\mu\left[\frac{\partial u^{n'}}{\partial x^{i'}}(g)^{1/2}g^\ell_{(n')}+\frac{\partial u^{i'}}{\partial x^{n'}}(g)^{1/2}g^\ell_{(n')}\right]\Big\}_{,\ell}=0 \tag{4b}$$

energy

$$[(g)^{1/2}\rho E]_{,t}+\Big\{(\rho E+p)\underline{u}\cdot(g)^{1/2}\underline{g}^\ell$$
$$-\frac{\gamma M_\infty}{Re}\frac{\mu}{Pr}\frac{\partial e_i}{\partial x^{i'}}(g)^{1/2}g^\ell_{(i')}-\frac{M_\infty\lambda}{Re}\,\mathrm{div}\ \underline{uu}\cdot(g)^{1/2}\underline{g}^\ell$$
$$-\frac{M_\infty\mu}{Re}\left[u^{m'}\frac{\partial u^{m'}}{\partial x^{k'}}(g)^{1/2}g^\ell_{(k')}+u^{m'}\frac{\partial u^{n'}}{\partial x^{m'}}(g)^{1/2}g^\ell_{(n')}\right]\Big\}_{,\ell}=0 \tag{4c}$$

where $g^\ell_{(i')}$ is the component of the contravariant base vector $\underline{g}^\ell$ in the $x^{i'}$ direction [i.e., $\underline{g}^\ell=(\partial x^\ell/\partial x^{i'})\underline{g}_{i'}=g^\ell_{(i')}\underline{g}_{i'}$] and $\underline{g}_{i'}$ is the Cartesian unit base vector. Note that in a finite difference approach, $(g)^{1/2}$ is factored out in the spatial derivative term. In the present formulation the $(g)^{1/2}$ is kept with $\underline{g}^\ell$ for an easy physical interpretation.

The above system of equations is valid for turbulent as well as laminar flow by replacing the molecular transport coefficients with their turbulent counterparts

$$\mu\Rightarrow\mu_\ell+\mu_t \tag{5a}$$

$$\frac{\mu}{Pr}\Rightarrow\frac{\mu_\ell}{Pr_\ell}+\frac{\mu_t}{Pr_t} \tag{5b}$$

where μ_t represents the turbulent eddy viscosity and Pr_t the turbulent Prandtl number. There should be no confusion when Eq. (5a) is used in the viscous stress terms and Eq. (5b) is used in the heat conduction terms. Sutherland's formula to evaluate the molecular viscosity, plus a turbulence model, closes the system of governing equations. A two-layer turbulence model developed by Baldwin and Lomax[2] with a "modified distance" as described in Ref. 10 is used.

Finite-Volume Formulation

A finite volume, indexed by (i,j,k), is prescribed by eight corner points connected with straight lines, as shown in Fig. 1. The edges of the cell define the nonorthogonal coordinate directions x^i, (ξ,η,ζ), and the bonding surface consists of a family of three pairs of coordinate surfaces that delineate the hexahedronal mesh cell. Note that, for $d\mathcal{V}=(g)^{1/2}\Delta x^1\Delta x^2\Delta x^3$ and $\Delta x^1=\Delta x^2=\Delta x^3=1$ in Eq. (2), $(g)^{1/2}$ is the volume of computational cell $d\mathcal{V}(i,j,k)$, the term $(g)^{1/2}\underline{g}^\ell$ denotes the vector for the surface $x^\ell=$ const, and $\underline{u}\cdot\underline{g}^\ell$ is the corresponding contravariant velocity. Therefore, in Eqs. (4a-c), $(g)^{1/2}g^\ell_{(i')}$ is the surface area for $x^\ell=$ const projected on the Cartesian coordinate of $x^{i'}=$ const.

In a finite difference approach, $(g)^{1/2}$ and $(g)^{1/2}\underline{g}^\ell$ are presented at each grid point, and are typically evaluated by a two-point central difference in all three directions. This leads to an inconsistency in the volume and surface calculations such that the geometry conservation law is not satisfied and, hence, the difference scheme cannot recapture the freestream. This inconsistency does not occur in the present approach.

Note that any open-surface element for a given boundary has a unique, effective surface vector $\underline{S}$ that is independent of the shape of the surface. This is because, by applying the divergence theorem to a constant vector, the integral of the outward-oriented surface normal over a closed surface vanishes

$$\int_S \phi\underline{n}\,dS=\int_{\mathcal{V}}\nabla\phi\,d\mathcal{V}=0 \quad \text{for } \phi=\text{const}$$

For instance, the surface vector $\underline{S}_{5678}$ in Fig. 1 is independent of the choice of which partitioning surface diagonal is used to define the cell volume (see next paragraph). Indeed, whether the four vertices are on a plane or not, the surface vector is equal to one-half the cross product of its diagonal line segments (see Ref. 11).

$$\underline{S}_{5678}=0.5(\underline{r}_{75}\times\underline{r}_{85}+\underline{r}_{65}\times\underline{r}_{75})=0.5(\underline{r}_{75}\times\underline{r}_{86})$$

Given eight arbitrary corner points prescribing a general hexahedron, a simple way to define a shape whose volume can be precisely calculated is to partition each face into two planar triangles. The volume is then dependent on which diagonal is used on each face, since the diagonals of four nonplanar points do not intersect. In order for neighboring cells to be contiguous, without gaps or overlaps, neighboring cell faces must have the same surface partitioning. A simple and consistent method for calculating cell volume, recently developed by Kordulla and Vinokur,[11] is given as

$$\begin{aligned}6\,\text{Vol}&=\underline{r}_{71}\cdot[(\underline{r}_{31}\times\underline{r}_{21})+(\underline{r}_{21}\times\underline{r}_{81})+(\underline{r}_{41}\times\underline{r}_{31})\\&\quad+(\underline{r}_{61}\times\underline{r}_{41})+(\underline{r}_{51}\times\underline{r}_{61})+(\underline{r}_{81}\times\underline{r}_{51})]\\&=\underline{r}_{71}\cdot[(\underline{r}_{31}\times\underline{r}_{24})+(\underline{r}_{81}\times\underline{r}_{52})+(\underline{r}_{61}\times\underline{r}_{45})]\\&=2\underline{r}_{71}\cdot(\underline{S}_{1432}+\underline{S}_{1285}+\underline{S}_{1465})\end{aligned}$$

With the volume and surface evaluated in the integral form, Eq. (1) can be discretized as

$$d\mathcal{V}_{i,j,k}\frac{\Delta\underline{q}_{i,j,k}}{\Delta t}+\delta[(\underline{q}\underline{u}+\underline{b})\cdot\underline{S}]_{i,j,k}=0 \qquad (6)$$

where $\underline{q}_{i,j,k}$ is now interpreted as the volumetric average located at the center of the cell and $(\underline{q}\underline{u}+\underline{b})\cdot\underline{S}$ is the corresponding flux evaluated at the surface $\underline{S}$. In the present study, the discretized finite-volume formulation, Eq. (6), is used for computation. In later discussions, for the purpose of explanation, Eq. (2) will be used. However, details of terms which have to be evaluated for carrying out calculations are based on Eqs. (4a-c), with corresponding interpretations of $(g)^{1/2}$ as the volume at the centroid and $(g)^{1/2}\underline{g}^\ell$ as the surface vector at the boundary of each finite-volume cell. The remaining quantities, such as contravariant and covariant base vectors, can be derived accordingly.

As one can see, the formulation does not require a global coordinate transformation. In fact, the only data needed concerning the mesh are the three Cartesian coordinates of the eight vertices of every cell in the mesh system. Moreover, the surface and volume of each cell are well defined and consistently evaluated, in contrast to a finite difference approach where the transformation coefficient and the Jacobian are evaluated from surrounding points.

In a finite-volume formulation, only the cell volume $(g)^{1/2}$ and the surface normal $(g)^{1/2}\underline{g}^\ell$ are needed for an inviscid flow calculation. To evaluate the viscous terms, the distance between two neighboring mesh cells is needed. In the present study, instead of calculating this distance from the centroids of two adjacent cells, the vector between cells, say (i,j,k) and $(i+1,\ j,k)$ (see Fig. 2), is set in the same direction as $\underline{S}_b$ (normal to the surface S_b), and is evaluated by

$$\underline{d}_{i,j,k}\cdot\underline{S}_b=|\underline{d}_{i,j,k}|\,|\underline{S}_b|=0.5(g^{1/2}_{i+1,j,k}+g^{1/2}_{i,j,k}) \qquad (7)$$

When shape variations are large, a more appropriate formula (not used herein) is

$$\begin{aligned}\underline{d}_{i,j,k}\cdot(\underline{S}_a+2\underline{S}_b+\underline{S}_c)&=|\underline{d}_{i,j,k}|\,|\underline{S}_a+2\underline{S}_b+\underline{S}_c|\\&=2(g^{1/2}_{i+1,j,k}+g^{1/2}_{i,j,k})\end{aligned}$$

This implies that in a viscous dominated region, for example near the wall, the grid would be required to be nearly orthogonal for an accurate calculation of the viscous term. For a highly skewed grid, an alternate method of evaluating $\underline{d}_{i,j,k}$ is needed (e.g., centroid difference).

Thin-Layer Approximation

For high Reynolds number flows the viscous effects are confined to a region near the wall boundary and are dominated by the viscous terms associated with the strain rates normal to the wall. The viscous terms with the strain rates along the body are comparatively small and insignificant. This concept was first discussed by Prandtl in the development of boundary-layer theory, and has been applied and extended to various problems. The development of the thin-layer approximation by Baldwin and Lomax[2] is based on this concept, with the retention of unsteady terms and all of the inviscid terms of the Navier-Stokes equations. Here, the concept is extended to thin layers in all three directions for a general coordinate system. All of the viscous terms associated with cross derivatives $\partial^2/\partial x^i\partial x^j$ when $i\neq j$ are neglected, while retaining the terms with normal second derivatives $\partial^2/\partial x^i\partial x^j$ when $i=j$, in each direction. For instance, for each x^2

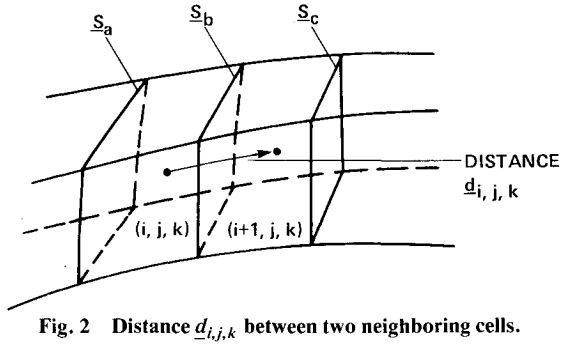

Fig. 2 Distance $\underline{d}_{i,j,k}$ between two neighboring cells.

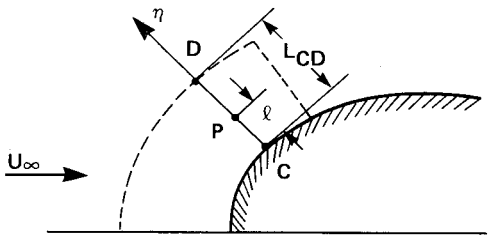

Fig. 3 Region near the nose for setting starting conditions.

direction the λ div $\underline{u}$ term in Eq. (4b) would be:

$$\frac{\partial}{\partial x^2}\left[\ldots\lambda\frac{\partial u^{n'}}{\partial x^{n'}}(g)^{1/2}g^2_{(i')}+\ldots\right]=\frac{\partial}{\partial x^2}\left[\lambda(g)^{1/2}g^2_{(i')}\right.$$

$$\times\Bigg(\underbrace{\frac{\partial u^{1'}}{\partial x^1}\frac{\partial x^1}{\partial x^{1'}}+\frac{\partial u^{2'}}{\partial x^1}\frac{\partial x^1}{\partial x^{2'}}+\frac{\partial u^{3'}}{\partial x^1}\frac{\partial x^1}{\partial x^{3'}}}_{\text{neglected}}\underbrace{+\frac{\partial u^{1'}}{\partial x^2}\frac{\partial x^2}{\partial x^{1'}}+\frac{\partial u^{2'}}{\partial x^2}\frac{\partial x^2}{\partial x^{2'}}+\frac{\partial u^{3'}}{\partial x^2}\frac{\partial x^2}{\partial x^{3'}}}_{\text{retained}}\underbrace{+\frac{\partial u^{1'}}{\partial x^3}\frac{\partial x^3}{\partial x^{1'}}+\frac{\partial u^{2'}}{\partial x^3}\frac{\partial x^3}{\partial x^{2'}}+\frac{\partial u^{3'}}{\partial x^3}\frac{\partial x^3}{\partial x^{3'}}}_{\text{neglected}}\Bigg)+\ldots\Bigg]$$

$$\approx\frac{\partial}{\partial x^2}\left[\ldots+\lambda(g)^{1/2}g^2_{(i')}\left(\frac{\partial u^{1'}}{\partial x^2}\frac{\partial x^2}{\partial x^{1'}}+\frac{\partial u^{2'}}{\partial x^2}\frac{\partial x^2}{\partial x^{2'}}+\frac{\partial u^{3'}}{\partial x^2}\frac{\partial x^2}{\partial x^{3'}}\right)+\ldots\right]$$

or for each x^ℓ direction

$$\frac{\partial}{\partial x^\ell}\left[\ldots\lambda\frac{\partial u^{n'}}{\partial x^{n'}}(g)^{1/2}g^\ell_{(i')}+\ldots\right]\approx\frac{\partial}{\partial x^\ell}\left[\ldots\lambda\frac{\partial u^{n'}}{\partial x^\ell}\frac{\partial x^\ell}{\partial x^{n'}}(g)^{1/2}g^\ell_{(i')}+\ldots\right]$$

(summation in n' and no summation in ℓ)

(8)

The terms $\partial x^\ell/\partial x^{n'}$ are evaluated as described in Eq. (7). This approximation drastically simplifies the evaluation of the viscous terms.

It is worthwhile to point out a difference in the evaluation of viscous terms by a finite difference method relative to the present approach. Consider the product $(\partial x^\ell/\partial x^{n'})g^\ell_{(i')}$ that occurs in Eq. (8) for the case when $n'=i'$. In a finite difference method [see Eq. (9) of Ref. 12] this product would be the square of a transformation coefficient (e.g., ξ_z^2 for $\ell=3$ and $i'=3$). In the present approach, $\partial x^\ell/\partial x^{n'}$ is evaluated from Eq. (7) and approximates the inverse of the distance between cells, whereas $g^\ell_{(i')}$ is determined by the geometry of the surface between the two cells involved.

It should be noted that not all of the terms retained are larger than the terms neglected. Retention of all of the second-order normal derivative terms makes the approximation convenient and consistent such that all dominant terms are retained for a general coordinate system, except near the juncture of two walls. Very near the juncture of two or more walls, the neglected cross derivatives can be of the same order of magnitude as the retained normal derivatives. But the flow contains comparatively very low momentum there and, therefore, the neglect of cross derivatives will not significantly affect the general features of the flowfield.

When not needed (because of the absence of a thin viscous layer), the viscous terms in any individual direction can be neglected completely, and the present algorithm will reduce back to a thin-layer approximation for the existence of viscous layers in two or only one direction.

Locally One-Dimensional Time Splitting

The concept of splitting, commonly known as the method of alternating directions, has been widely used to transform complex operators into a sequence of simpler ones. This concept is applied here to reduce the set of three-dimensional equations, Eq. (2), into three sets of one-dimensional equations.

Equation (2) can be split into three locally one-dimensional (LOD) operators as

$$Lx:\ \hat{\underline{q}}_{,t}+{}^i\hat{\underline{F}}_{,i}=0\ \text{(no summation in } i)\quad i=1,2,3 \tag{9}$$

Here, each of the split operators contains the spatial derivatives of flux in only one direction. Since this discussion is limited to the LOD scheme, the summation convention will not be used in this section.

Let Δt be the time step, n the time level, and ${}^i\hat{\underline{F}}$ the flux across the cell surface $x^i=\text{const}$. The LOD predictor-corrector explicit-implicit scheme can be expressed as follows:

Predictor

$$\text{explicit}\quad \Delta\hat{\underline{q}}^n=-\Delta t\left(\frac{\Delta_+\,{}^i\hat{\underline{F}}}{\Delta x^i}\right)$$

$$\text{implicit}\quad \left(I-\Delta t\frac{\Delta_+\,|{}^i\hat{\underline{\underline{A}}}|^n\cdot}{\Delta x^i}\right)\overline{\delta\hat{\underline{q}}^{n+1}}=\Delta\hat{\underline{q}}^n$$

$$\text{update}\quad \overline{\hat{\underline{q}}^{n+1}}=\hat{\underline{q}}^n+\overline{\delta\hat{\underline{q}}^{n+1}} \tag{10a}$$

Corrector

$$\text{explicit}\quad \overline{\Delta\hat{\underline{q}}^{n+1}}=-\Delta t\left(\frac{\Delta_-\,{}^i\hat{\underline{F}}}{\Delta x^i}\right)$$

$$\text{implicit}\quad \left(I+\Delta t\frac{\Delta_-\,\overline{|{}^i\hat{\underline{\underline{A}}}|^{n+1}}\cdot}{\Delta x^i}\right)\delta\hat{\underline{q}}^{n+1}=\overline{\Delta\hat{\underline{q}}^{n+1}}$$

$$\text{update}\quad \hat{\underline{q}}^{n+1}=\tfrac{1}{2}(\hat{\underline{q}}^n+\overline{\hat{\underline{q}}^{n+1}}+\delta\hat{\underline{q}}^{n+1}) \tag{10b}$$

Here, the overbars in the corrector sweeps indicate that the quantities are determined with updated predictor values. The Δ_+ and Δ_- indicate the forward and backward two-point differences. The matrices $|{}^i\hat{\underline{\underline{A}}}|$ are matrices with positive eigenvalues

$$|{}^i\hat{\underline{\underline{A}}}|=\hat{M}_i^{-1}(\,|{}^i\underline{\underline{D}}|\,)\hat{M}_i$$

where

$$|{}^i\underline{\underline{D}}|=\begin{bmatrix}{}^i\lambda_1 & & & & 0\\ & {}^i\lambda_2 & & & \\ & & {}^i\lambda_3 & & \\ & & & {}^i\lambda_4 & \\ 0 & & & & {}^i\lambda_5\end{bmatrix}$$

The $\hat{M}_i$ are the similarity transformation matrices which diagonalize the Eulerian Jacobian ${}^i\hat{\underline{\underline{A}}}$ in Eq. (3) with $\mu=\lambda=0$. In $|{}^i\underline{\underline{D}}|$, there are three distinct representative eigenvalues, defined by

$${}^i\lambda_u=\max\left(|\underline{u}\cdot\underline{g}^i|+\frac{2\mu\gamma M_\infty}{RePr}\frac{g^{ii}}{\rho\Delta x^i}-\frac{\Delta x^i}{\Delta t},\ 0\right)$$

$${}^i\lambda_{u\pm a}=\max\left[|\underline{u}\cdot\underline{g}^i\pm a(g^{ii})^{1/2}|+\frac{2\mu\gamma M_\infty}{RePr}\frac{g^{ii}}{\rho\Delta x^i}-\frac{\Delta x^i}{\Delta t},\ 0\right]$$

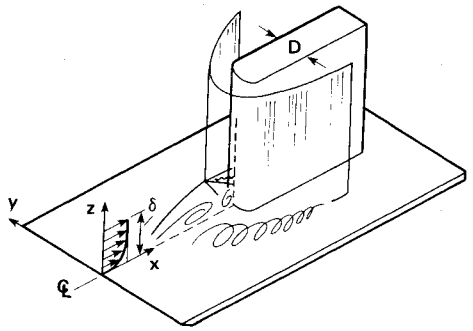

Fig. 4 Blunt fin on a flat plate.

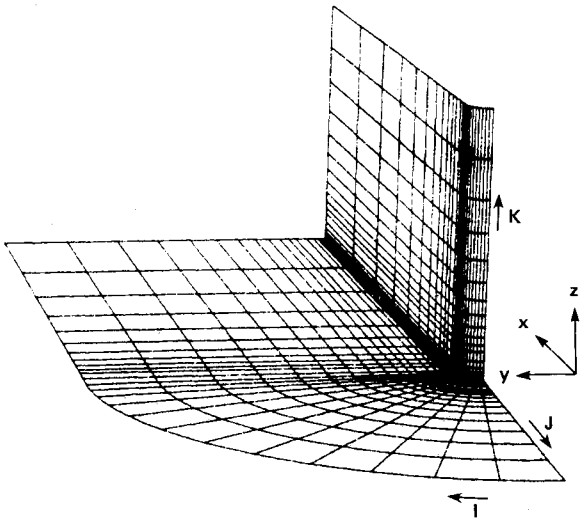

Fig. 5 Mesh distribution on the blunt fin and the flat plate.

for $i=1$ $\quad {}^{1}\lambda_1={}^{1}\lambda_3={}^{1}\lambda_4={}^{1}\lambda_u$

$${}^{1}\lambda_2={}^{1}\lambda_{u+a},\ \text{and}\ {}^{1}\lambda_5={}^{1}\lambda_{u-a}$$

for $i=2$ $\quad {}^{2}\lambda_1={}^{2}\lambda_2={}^{2}\lambda_4={}^{2}\lambda_u$

$${}^{2}\lambda_3={}^{2}\lambda_{u+a},\ \text{and}\ {}^{2}\lambda_5={}^{2}\lambda_{u-a}$$

for $i=3$ $\quad {}^{3}\lambda_1={}^{3}\lambda_2={}^{3}\lambda_3={}^{3}\lambda_u$

$${}^{3}\lambda_4={}^{3}\lambda_{u+a},\ \text{and}\ {}^{3}\lambda_5={}^{3}\lambda_{u-a}$$

where

$$g^{ii}=\underline{g}^{i}\cdot\underline{g}^{i}$$

Each transformation matrix of $\hat{M}_i$ $(i=1,2,3)$ is split into three matrices

$$\hat{M}_i=M_{iC}M_{iT}M$$

where

$$M=\begin{bmatrix} 1 & 0 & 0 & 0 & 0 \\ -u\rho^{-1} & \rho^{-1} & 0 & 0 & 0 \\ -v\rho^{-1} & 0 & \rho^{-1} & 0 & 0 \\ -w\rho^{-1} & 0 & 0 & \rho^{-1} & 0 \\ \alpha\beta & -\beta u & -\beta v & -\beta w & \beta \end{bmatrix}$$

$$\alpha=0.5(u^2+v^2+w^2)\ \text{and}\ \beta=(\gamma-1)$$

for $i=1$

$$M_{1C}=\begin{bmatrix} 1 & 0 & 0 & 0 & -a^{-2} \\ 0 & \rho a & 0 & 0 & 1 \\ 0 & 0 & 1 & 0 & 0 \\ 0 & 0 & 0 & 1 & 0 \\ 0 & -\rho a & 0 & 0 & 1 \end{bmatrix}$$

$$M_{1T}=\begin{bmatrix} 1 & 0 & 0 & 0 & 0 \\ 0 & e^{1}_{(1')} & e^{1}_{(2')} & e^{1}_{(3')} & 0 \\ 0 & -e^{1}_{(2')} & e^{1}_{(1')} & 0 & 0 \\ 0 & -e^{1}_{(3')} & 0 & e_{(1')} & 0 \\ 0 & 0 & 0 & 0 & 1 \end{bmatrix}$$

for $i=2$

$$M_{2C}=\begin{bmatrix} 1 & 0 & 0 & 0 & -a^{-2} \\ 0 & 1 & 0 & 0 & 0 \\ 0 & 0 & \rho a & 0 & 1 \\ 0 & 0 & 0 & 1 & 0 \\ 0 & 0 & -\rho a & 0 & 1 \end{bmatrix}$$

$$M_{2T}=\begin{bmatrix} 1 & 0 & 0 & 0 & 0 \\ 0 & e^{2}_{(2')} & -e^{2}_{(1')} & 0 & 0 \\ 0 & e^{2}_{(1')} & e^{2}_{(2')} & e^{2}_{(3')} & 0 \\ 0 & 0 & -e^{2}_{(3')} & e^{2}_{(2')} & 0 \\ 0 & 0 & 0 & 0 & 1 \end{bmatrix}$$

for $i=3$

$$M_{3C}=\begin{bmatrix} 1 & 0 & 0 & 0 & -a^{2} \\ 0 & 1 & 0 & 0 & 0 \\ 0 & 0 & 1 & 0 & 0 \\ 0 & 0 & 0 & \rho a & 1 \\ 0 & 0 & 0 & -\rho a & 1 \end{bmatrix}$$

$$M_{3T}=\begin{bmatrix} 1 & 0 & 0 & 0 & 0 \\ 0 & e^{3}_{(3')} & 0 & -e^{3}_{(1')} & 0 \\ 0 & 0 & e^{3}_{(3')} & -e^{3}_{(2')} & 0 \\ 0 & e^{3}_{(1')} & e^{3}_{(2')} & e^{3}_{(3')} & 0 \\ 0 & 0 & 0 & 0 & 1 \end{bmatrix}$$

Here, $e^{l}_{(i')}=g^{l}_{(i')}/(g^{ll})^{1/2}$ is the component of the normalized contravariant vector in the i' direction. The M matrix transforms $\delta\underline{q}$ from conservative to nonconservative variables [i.e., from $(\delta\rho, \delta\rho u, \delta\rho v, \delta\rho w, \delta\rho E)$ to $(\delta\rho, \delta u, \delta v, \delta w, \delta p)$], the matrices M_{iT} account for the orientation of the surfaces $x^i=\text{const}$, and the matrices M_{iC} then transform from nonconservative to characteristic forms. Comparing the $\hat{M}_i$ matrices with those similarity transformation matrices given in Ref. 1, one can see that the matrices M and M_{iC} are the same in the orthogonal Cartesian coordinates and the nonorthogonal curvilinear coordinate systems; the matrices M_{iT} introduce the generalized coordinate transformation. The

characteristic variables are:

for $i=1$

$$\delta\hat{Q}_{1C}=\begin{bmatrix}\delta\rho-(1/a^2)\delta p\\ \delta p+\rho a\delta\underline{u}\cdot\underline{g}^1/(g^{11})^{1/2}\\ e^1_{(1')}\delta v-e^1_{(2')}\delta u\\ e^1_{(1')}\delta w-e^1_{(3')}\delta u\\ \delta p-\rho a\delta\underline{u}\cdot\underline{g}^1/(g^{11})^{1/2}\end{bmatrix}$$

for $i=2$

$$\delta\hat{Q}_{2C}=\begin{bmatrix}\delta\rho-(1/a^2)\delta p\\ e^2_{(2')}\delta u-e^2_{(1')}\delta v\\ \delta p+\rho a\delta\underline{u}\cdot\underline{g}^2/(g^{22})^{1/2}\\ e^2_{(2')}\delta w-e^2_{(3')}\delta v\\ \delta p-\rho a\delta\underline{u}\cdot\underline{g}^2/(g^{22})^{1/2}\end{bmatrix}$$

for $i=3$

$$\delta\hat{Q}_{3C}=\begin{bmatrix}\delta\rho-(1/a^2)\delta p\\ e^3_{(3')}\delta u-e^3_{(1')}\delta w\\ e^3_{(3')}\delta v-e^3_{(2')}\delta w\\ \delta p+\rho a\delta\underline{u}\cdot\underline{g}^3/(g^{33})^{1/2}\\ \delta p-\rho a\delta\underline{u}\cdot\underline{g}^3/(g^{33})^{1/2}\end{bmatrix}$$

Now it is clear that $\hat{M}_i$ transforms the inviscid portion of ${}^j\hat{F}_j$ into characteristic form $\delta\hat{Q}_{jC}$ *only* when $i=j$. This implies that, in contrast to the unsplit formulation, the LOD splitting makes the inviscid portion of the right-hand-side dependent variables consistent with the characteristic variables by means of the similarity transformation employed in the implicit steps, Eqs. (10a) and (10b).

Two points should be noted here. First, to develop a similarity transformation for each entire viscous Jacobian ${}^i\hat{\bar{A}}$ is an insurmountable task. To keep the right-hand sides of Eqs. (10a) and (10b) as simple and straightforward as possible, we here follow the suggestion of MacCormack[1] to consider only the Eulerian Jacobian of ${}^i\hat{\bar{A}}$, with the addition of a small number of dominant viscous terms to the Eulerian eigenvalues. Second, the implicit procedure is skipped whenever the explicit stability conditions are satisfied locally, and the algorithm requires virtually no more computation time than an explicit method.

Each Lx^i operator described above consists of an explicit-implicit predictor-corrector set, and is second-order accurate in time and space, unconditionally stable, and requires no block or scalar tridiagonal inversion, as discussed in Ref. 1. Because of the noncommutativity of Lx^i operators, the simple combined numerical scheme $Lx^1Lx^2Lx^3$ is only of first order. To retain the second-order accuracy of the method, a symmetric sequence of the LOD operators, developed by Strang,[8] is used. Here, we have the complete numerical procedure expressed as

$$\hat{\underline{q}}^{n+2}=L\eta(\Delta t)L\zeta(\Delta t)L\xi(2\Delta t)L\zeta(\Delta t)L\eta(\Delta t)\hat{\underline{q}}^n$$

by which the solution is advanced two time steps from t to $t+2\Delta t$. Each locally one-dimensional operator is applied line by line in each sweep direction and, hence, only needs one level plus three single arrays of dependent variables. Without this splitting, the MacCormack scheme requires, in general, two time levels of variables plus a level of right-hand-side residuals for a total of three levels of variables stored.

Boundary Conditions

Boundary conditions to be imposed are problem dependent. For the test problem of supersonic flow over a blunt fin at zero angle of attack, an incoming boundary-layer profile is prescribed along the outer boundary of the flat plate. The fin is assumed infinite in height and length, so that zero-gradient boundary conditions may be used in each corresponding direction. On the plane of symmetry, a symmetry condition is imposed. The wall is assumed impermeable, and no-slip boundary conditions are applied. The wall is also taken to be adiabatic. The pressure has a zero gradient normal to the wall. These boundary conditions are imposed at the beginning of each sweep. The wall flux is cancelled immediately after the predictor step, and not carried over to the corrector step as suggested in Ref. 1.

Blunt-Body Starting Conditions

The simplest way to start a computational process is by assuming that all initial conditions are the same as the incoming flow conditions. This very often leads to overcompression near the stagnation region, followed by an overexpansion around the shoulder. The overexpansion may result in a negative density which makes the numerical scheme unstable. To avoid this, Pulliam and Steger[12] used a small time increment at the start-up stage and a so-called "soft start" by gradually imposing the no-slip wall condition. Rizk et al.[13] treated the bow shock as a discontinuity and started with an assumed shock shape and a Newtonian pressure distribution, in addition to the soft-start techniques. With walls in more than one direction and the existence of boundary layers on the wall, the bow shock cannot be fixed. In this study a simple device is employed to avoid the overexpansion. As sketched in Fig. 3, near the nose region the normal velocity component is set to zero on the body, say, at C, and then increased linearly to the incoming velocity at a preassigned location, say D. The formula for velocity at a point P in between is

$$\underline{u}_P=\underline{u}_D-(1-\ell/L_{CD})[(\underline{u}\cdot\underline{g}^\eta)\underline{g}^\eta/g^{\eta\eta}]_C$$

where L_{CD} is the length from C to D, and ℓ is the variable length from the surface. The density and energy are set equal

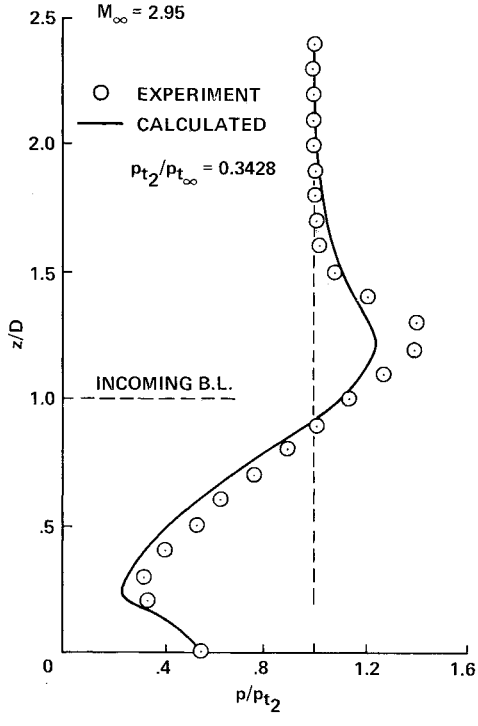

Fig. 6 Pressure on fin leading edge.

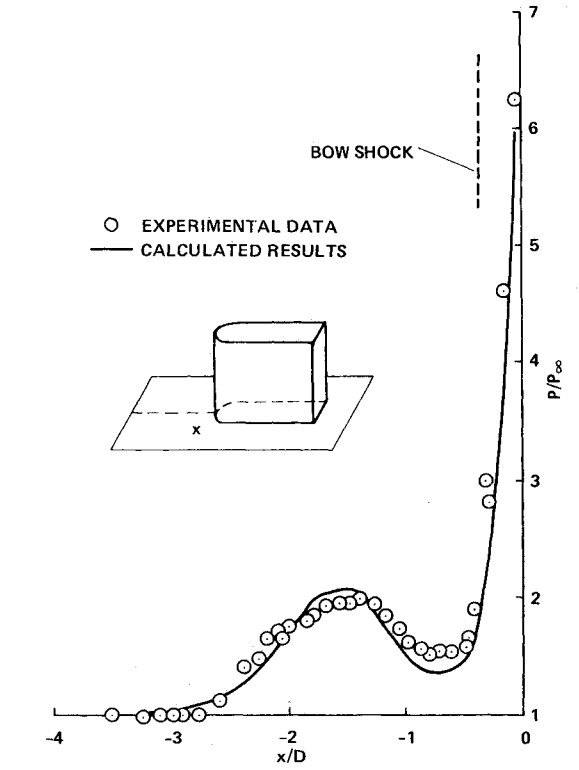

Fig. 7 Pressure on the flat plate along the line of symmetry ($y=0$).

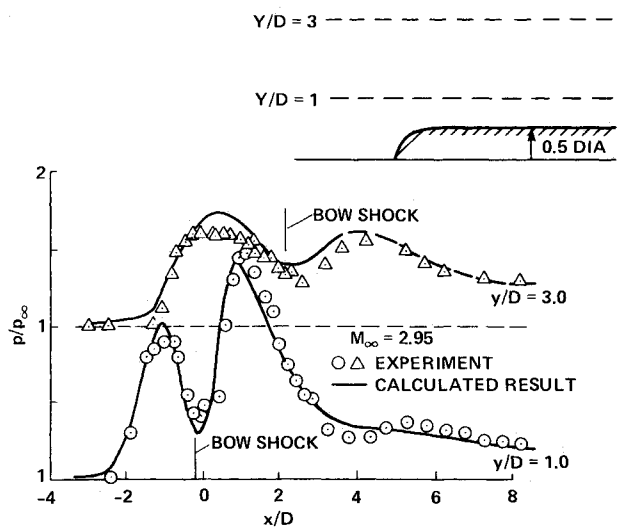

Fig. 8 Pressure on the flat plate along $y/D=1.0$ and 3.0.

to the incoming conditions. This simple technique may be interpreted as a defect of normal momentum and, hence, kinetic energy in a small region near the blunt nose. It alleviates the nonphysical flowfield development, and allows large time increments (or a large CFL number) during the start-up phase.

Results and Discussion

The LOD time-split technique has been tested for supersonic flows over a compression corner and a planar shock impinging on a cylinder. Our results (not shown here) are in very good agreement with these previous calculations.[14,15] Coding in general three-dimensional coordinates, the case of blunt-fin induced shock wave/turbulent boundary-layer interaction was calculated. The experiment was done by Dolling and Bogdonoff[9] for $M_\infty=2.95$, an incoming boundary-layer thickness of $\delta=1.27$ cm, over a blunt fin of diameter $D=1.27$ cm, and at zero angle of attack, as shown in Fig. 4. The Reynolds number based on freestream velocity and fin diameter, Re, is about 0.8×10^6.The fin bow shock causes the boundary layer to separate from the surface ahead of the fin and the shock wave emanating from the separated flow region impinges on the fin bow shock wave, resulting in a lambda-type shock pattern plus other complex structures. Figure 5 shows the (40,32,32) mesh system in which both the η and ζ directions are geometrically stretched. The size of the first mesh cell off the wall is equal to 0.00433 of the diameter of the fin to ensure sufficient resolution of the viscous effects near the wall. Figure 6 shows the comparison of static pressure along the fin leading-edge stagnation line. The agreement is very good. The location of peak pressure is closely predicted. This peak pressure would normally be attributed to the existence of Edney Type IV[16] interference (to be discussed later) between the fin bow shock and the separation shock. Extremely high heating rates associated with this type of interference have been observed in many experiments[17,18] and in supersonic flight. Comparisons of pressure on the flat plate along the centerline are shown in Fig. 7, and the pressures along the lines of $y/D=1$ and 3 in Fig. 8. Again the agreement is very good, and all of the main features, such as upstream influence, plateau pressure (Fig. 7), and double peaks of pressure (Fig. 8), are well simulated.

The particle path in the plane of symmetry (Fig. 9a) clearly shows the existence of a primary horseshoe vortex and a secondary separation (see the fine resolution in Fig. 9b). This three-dimensional spiral-vortex separated flowfield structure is drastically different from the well-studied, two-dimensional, concentric separation pattern as sketched in Fig. 10. In a two-dimensional recirculation (Fig. 10a) the separation point and reattachment point are connected by a $u=0$ velocity line and a dividing streamline. The region is closed and the streamlines inside are concentric. In a three-

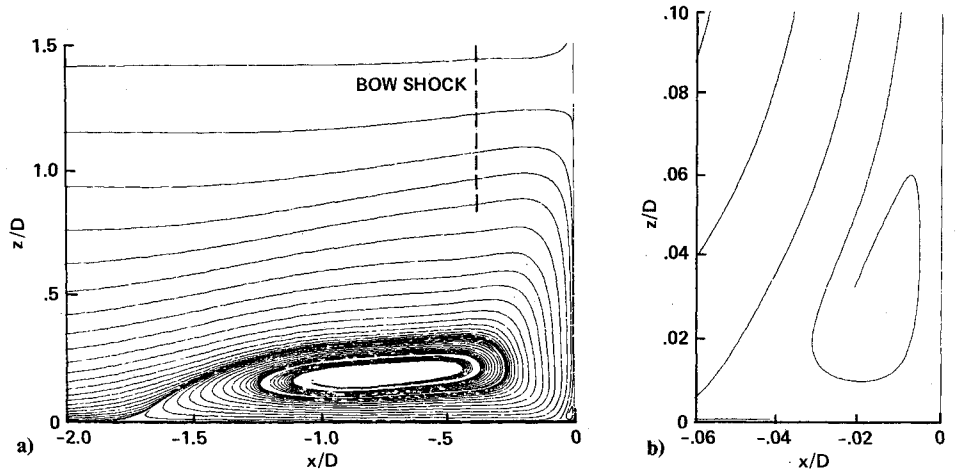

Fig. 9 Horseshoe vortex flowfield: a) particle paths on the plane of symmetry; b) details of secondary separation on the plane of symmetry.

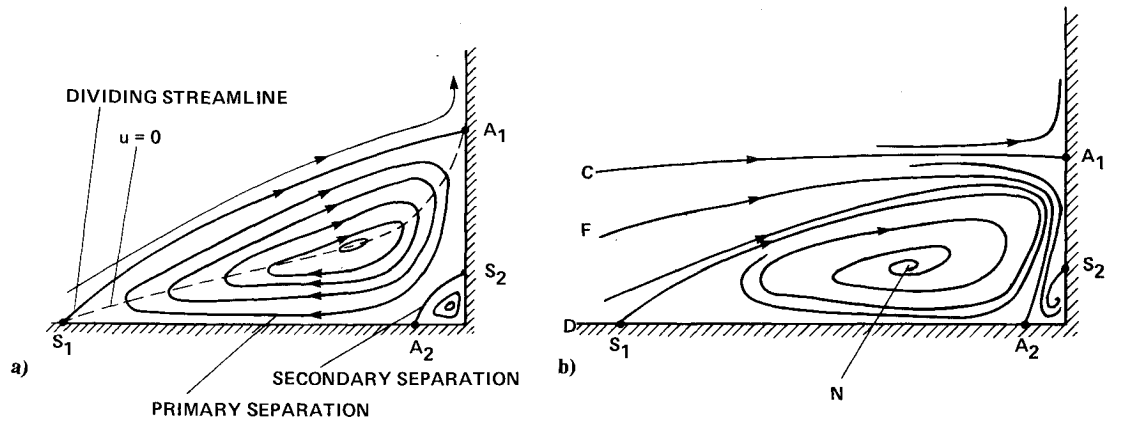

Fig. 10 Differences between two- and three-dimensional separations: a) two-dimensional separation; b) three-dimensional separation (on the plane of symmetry).

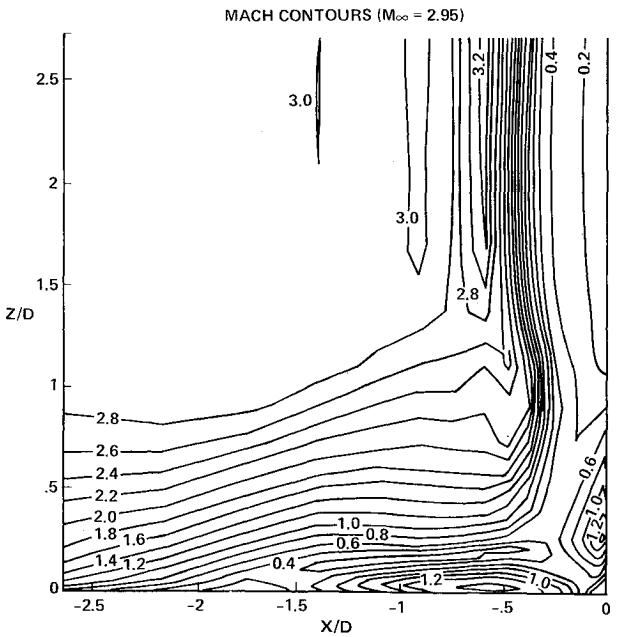

Fig. 11 Mach contours on the plane of symmetry.

dimensional separation (Figs. 9 and 10b), the separation and reattachment points cannot be connected by a streamline to form a closed vortex. As sketched in Fig. 10b, the flow between D and F is swept into the primary horseshoe vortex, and the high energy flow between C and F is swept into the secondary vortex.

Figure 11 shows a contour plot of Mach number in the plane of symmetry. Note that neither a strong Mach number variation nor a supersonic jet exists between the triple point of the lambda-shock and the fin, as expected in an Edney Type IV interference. At this Mach number the peak pressure observed in Fig. 7 might instead be purely due to multicompression. The most striking feature in Fig. 11 is the existence of two reversed-flow supersonic zones embedded in the subsonic recirculation region; one is under the horseshoe vortex on the flat plate and another is on the fin. The peak reversed supersonic Mach number is about 1.2 on the fin, and is above 1.45 on the flat plate. A similar feature (local supersonic zones) in three-dimensional separated flows was first experimentally observed by Voltenko et al.[19] for a supersonic stream at a Mach number of 3.11 over a cylinder mounted on a flat plate.

For the present test case with a (40,32,32) mesh and without any special effort at code vectorization, it takes about 4.8 s of CPU time on a Cray-1 computer for each time-step integration. It takes approximately 1.1 h for 800 time steps with a maximum CFL number of about 15 to reach a steady-state solution.

Concluding Remarks

A general-purpose computer code has been developed to solve the three-dimensional, compressible Navier-Stokes equations for high Reynolds number flows. The algorithm extends MacCormack's explicit-implicit scheme to a time-split, three-dimensional finite-volume concept in a general coordinate system. The thin-layer approximation in all three spatial directions drastically reduces the evaluation of viscous terms and allows the algorithm to solve more complicated geometries with wall boundaries in two or all three directions. A supersonic turbulent flow over a blunt fin mounted on a flat plate has been numerically simulated. Observations of the existence of peak pressure, primary horseshoe and secondary vortices, and reversed supersonic zones demonstrate that computational fluid dynamics can effectively supplement the wind tunnel tests for aerodynamic design as well as for understanding basic fluid dynamics.

References

[1] MacCormack, R. W., "A Numerical Method for Solving the Equations of Compressible Viscous Flow," *AIAA Journal*, Vol. 20, Sept. 1982, pp. 1275-1281.

[2] Baldwin, B. S. and Lomax, H., "Thin Layer Approximation and Algebriac Model for Separated Turbulent Flows," AIAA Paper 78-257, Jan. 1978.

[3] Hung, C. M. and Kurasaki, S. S., "Thin-Layer Approximation for Three-Dimensional Supersonic Corner Flows," *AIAA Journal*, Vol. 18, Dec. 1980, pp. 1544-1546.

[4] Coakley, T. J., "Numerical Method for Gas Dynamics Combining Characteristic and Conservation Concepts," AIAA Paper 81-1257, June 1981.

[5] Rizzi, A., "Damped Euler-Equations Method to Compute Transonic Flow Around Wing-Body Combinations," *AIAA Journal*, Vol. 20, Oct. 1982, pp. 1321-1328.

[6] MacCormack, R. W., "The Effect of Viscosity in Hypervelocity Impact Cratering," AIAA Paper 69-354, April 1969.

[7] Kordulla, W. and MacCormack, R. W., "Transonic-Flow Computation Using an Explicit-Implicit Method," *Lecture Notes in Physics*, Vol. 170, Springer-Verlag, June 1982, pp. 286-295.

[8] Strang, G., "On the Construction and Comparision of Difference Schemes," *SIAM Journal of Numerical Analysis*, Vol. 5, 1968, pp. 506-517.

[9] Dolling, D. S. and Bogdonoff, S. M., "Blunt Fin-Induced Shock Wave/Turbulent Boundary-Layer Interaction," *AIAA Journal*, Vol. 20, Dec. 1982, pp. 1674-1680.

[10] Hung, C. M. and MacCormack, R. W., "Numerical Solution of Three-Dimensional Shock Wave and Turbulent Boundary-Layer Interaction," *AIAA Journal*, Vol. 16, Oct. 1978, pp. 1090-1096.

[11]Kordulla, W. and Vinokur, M., "Efficient Computation of Volume in Flow Predictions," *AIAA Journal*, Vol. 21, June 1983, pp. 917-918.

[12]Pulliam, T. H. and Steger, J. L., "Implicit Finite-Difference Simulations of Three-Dimensional Compressible Flow," *AIAA Journal*, Vol. 18, Feb. 1980, pp. 159-167.

[13]Rizk, Y. M., Chaussee, D. S., and McRae, D. S., "Numerical Simulation of Viscous-Inviscid Interactions on Indented Nose Tips," AIAA Paper 82-0290, Jan. 1982.

[14]Hung, C. M. and MacCormack, R. W., "Numerical Simulation of Supersonic and Hypersonic Turbulent Compression Corner Flows," *AIAA Journal*, Vol. 15, March 1977, pp. 410-416.

[15]Hung, C. M., "Impingement of an Oblique Shock Wave on a Cylinder," *Journal of Spacecraft and Rockets*, Vol. 20, May-June 1983, pp. 201-206.

[16]Edney, B., "Anomalous Heat Transfer and Pressure Distributions on Blunt Bodies at Hypersonic Speeds in the Presence of an Impinging Shock," Aeronautical Research Institute of Sweden, Stockholm, Sweden, Rept. 115, Feb. 1968.

[17]Hiers, R. S. and Loubsky, W. J., "Effects of Shock-Wave Impingement on the Heat Transfer on a Cylindrical Leading Edge," NASA TN D-3859, Feb. 1967.

[18]Sedney, R. and Kitchens, C. W. Jr., "The Structure of Three-Dimensional Separated Flows in Obstacle-Boundary Layer Interactions," *Flow Separation*, AGARD CP-168, Paper 37, June 1975.

[19]Voltenko, D. M., Zubkov, A. I., and Panov, Yu. A., "The Existence of Supersonic Zones in Three-Dimensional Separated Flows," *Journal of Fluid Dynamics*, Vol. 2, No. 1, 1967, pp. 13-16.